International Tables for Crystallography (2006). Vol. C, Section 2.3.3.8, pp. 66–69.

the data by least squares in which the values of the derivatives can be calculated using a set of tabulated integers. The convolution range CR expressed as a multiple of the FWHM of the peak can be selected. A minimum of five points is required. For asymmetric peaks, such as occur at small 2θ's, a CR $\simeq$ 0.5 FWHM gives the best precision. The larger the CR the larger the intrinsic error but the smaller the random error, and the smaller the number of peaks identified in overlapping patterns. The larger CR also avoids false peaks in patterns with poor counting statistics. Fig. 2.3.3.8(*c*) shows the dependence of the accuracy of the peak determination on P/σ. The computer results list the 2θ's, d's, absolute and relative intensities (scaled to 100) of the identified peaks. The calculation is made with a selected wavelength such as $K\alpha_1$ and the possible $K\alpha_2$ peaks are flagged.

2.3.3.8. *Profile fitting*

Profile fitting has greatly advanced powder diffractometry by making it possible to calculate the intensities, peak positions, widths, and shapes of the reflections with a far greater precision than had been possible with manual measurements or visual inspection of the experimental data. The method has better resolution than the original data and the entire scattering distribution is used instead of only a few features such as the peak and width. Individual profiles and clusters of reflections can be fitted, or the entire pattern as in the Rietveld method (Chapter 8.6).

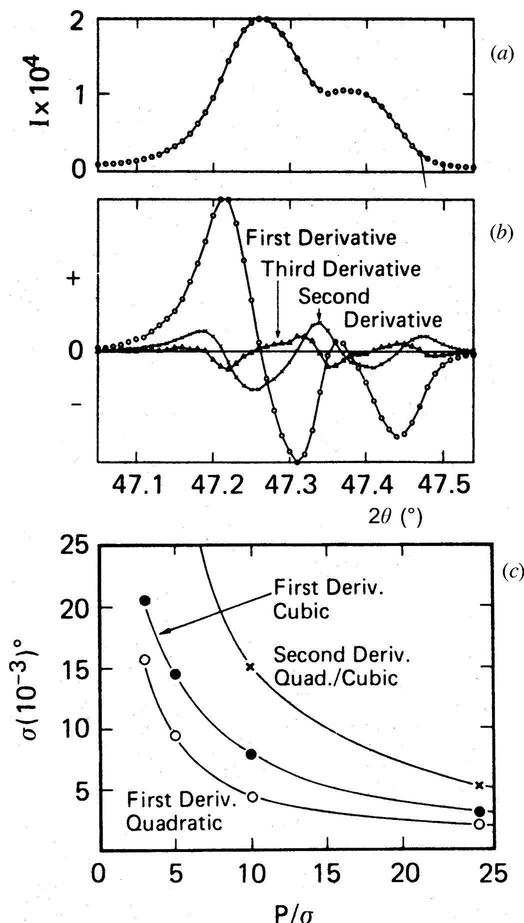

Fig. 2.3.3.8. (*a*) Si(220) Cu $K\alpha$ reflection. (*b*) First (circles), second (crosses), and third (triangles) derivatives of a seven-point polynomial of data in (*a*). (*c*) Average angular deviations as a function of P/σ for various derivatives.

The procedure is based on the least-squares fitting of theoretical profile intensities to the digitized powder pattern. The profile intensity at the ith step is calculated by

$$Y(x_i)_{\rm calc} = B(x_i) + \sum_j I_j P(x_i - T_j)_j, \qquad (2.3.3.12)$$

where $B(x_i)$ is the background intensity, I_j is the integrated intensity of the jth reflection, T_j is the peak-maximum position, $P(x_i)_j$ is the profile function to represent the profile shape, and $\sum_j$ is taken over j, in which the $P(x)_j$ has a finite value at x_i. Unlike the Rietveld method, a structure model is not used. In the least-squares fitting, I_j and T_j are refined together with background and profile shape parameters in $P(x)_j$. Smoothing the experimental data is not required because it underestimates the estimated standard deviations for the least-squares parameters, which are based on the counting statistics.

The experimental profiles are a convolution of the X-ray line spectrum λ and all the combined instrumental and geometrical

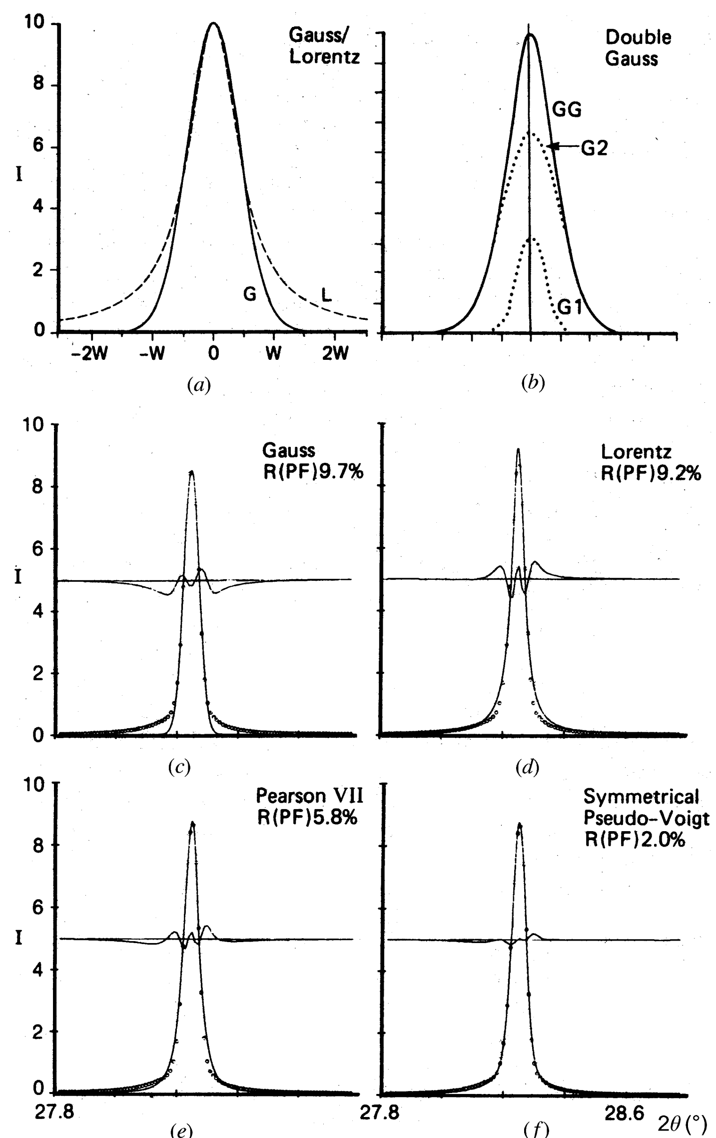

Fig. 2.3.3.9. (*a*) Computer-generated symmetrical Lorentzian profile L and Gaussian G with equal peak heights, 2θ and FWHM. (*b*) Double Gaussian GG shown as the sum of two Gaussians in which I and FWHM of $G1$ are twice those of $G2$ and 2θ is constant. (*c*)–(*f*) Profile fitting with different functions. Differences between experimental points and fitted profile shown at one-half height. Synchrotron radiation, Si(111).

Copyright © 2006 International Union of Crystallography

aberrations G with the true diffraction effects of the specimen S (Parrish, Huang & Ayers, 1976), *i.e.*

$$\Omega(x) = (\lambda * G) * S + \text{background}. \quad (2.3.3.13)$$

The profile shapes and resolution differ in the various diffractometer geometries and there is no universal profile-fitting function. In conventional X-ray tube focusing methods, the profiles are asymmetric and the shapes change continually across the scattering-angle range owing to the aberrations and the $K\alpha$ doublet. To avoid problems caused by the $K\alpha$ doublet, a few authors used the $K\beta$ line, but it has only about 1/7 the intensity. The profiles obtained with synchrotron radiation are symmetrical and narrower, and the widths increase with increasing 2θ. The different shapes and rates of decay of the tails make it necessary to find an analytical function that best fits the particular experimental profile. Langford (1987) and Young & Wiles (1982) have compiled and reviewed various profile-fitting functions and several are described below. Howard & Preston (1989) give details of the computations in their review of the method.

Early profile analyses used Gaussian or Lorentzian (Cauchy) curves. Fig. 2.3.3.9(*a*) shows that the most obvious difference is the rate of decay of the tails. X-ray synchrotron profiles lie between the two as shown in Figs. 2.3.3.9(*c*)–(*f*). The function must fit the tails as well as the main body and single-element functions are generally unsatisfactory. The Voigt function is a convolution of Lorenzian (L) and Gaussian (G) functions of different widths:

$$P(x)_V = \int L(x)G(x-u)\,\mathrm{d}u, \quad (2.3.3.14)$$

where x corresponds to $2\theta - T_j$ (Langford, 1978). It has been used for profile fitting and also to determine certain physical properties such as crystallite size and strain broadening from the constituent L and G profiles (see, for example, Langford, 1978; Suortti, Ahtee & Unonius, 1979; de Keijser, Langford, Mittemeijer & Vogels, 1982; Langford, Delhez, de Keijser & Mittemeijer, 1988). Evaluation of a symmetrical Voigt function involves the real part of the complex error function and an algorithm for calculating this has been given by Langford (1992).

The two most frequently used functions are at present the pseudo-Voigt (Wertheim, Butler, West & Buchanan, 1974) and the Pearson VII (Hall, Veeraraghavan, Rubin & Winchell, 1977). They cannot be easily deconvoluted analytically and have no direct physical interpretation but the equivalent Voigt parameters can be derived. Both can be split into symmetric and asymmetric portions to adjust better to the profile asymmetries and tails. The shapes can also be varied systematically by changing the L/G ratio (de Keijser, Langford, Mittemeijer & Vogels, 1982).

The pseudo-Voigt function is similar to the Voigt except that an addition is used in place of the convolution. It is easier to use and Wertheim *et al.* (1974) found there was only a small difference in the intensities and widths obtained with this approximation. It is defined as

$$P(x)_{\rm p-V} = \eta L(x) + (1-\eta)G(x), \quad (2.3.3.15)$$

where η is the ratio of Lorentz to Gauss and they have the same widths. The refined η and width of the full fitted profile can be related by a polynomial expansion (Hastings, Thomlinson & Cox, 1984; David, 1986; Cox, Toby & Eddy, 1988) to the widths of the L and G components of the original Voigt function. It is frequently used to fit synchrotron-radiation profiles. In the particular case shown in Figs. 2.3.3.9(*c*)–(*f*), the pseudo-Voigt has the best fit as shown by the difference curve at half-height and the lowest $R_p[= R(\mathrm{PF})]$ value.

The Pearson VII function is defined as

$$P(x)_{\rm PVII} = a[1 + (x/b)^2]^{-m}, \quad (2.3.3.16)$$

where m is a refinable parameter based on the G/L content (for $m = 1$, the curve is 100% Lorentzian and for $m = \infty$ it is 100% Gaussian), and $1/b = 2[2^{1/m} - 1]^{1/2}/W$, where W is the FWHM.

The peak asymmetry can be incorporated into the profile function in several ways. One is to multiply (or add) the symmetrical profile function with an asymmetric function (Rietveld, 1969). Another is to dispose two or three functions asymmetrically (Parrish, Huang & Ayers, 1976). A third is to use a split-type function, consisting of two profile functions, each of which defines one-half the total peak, *i.e.* the low- or high-angle sides of the peak and each has different profile widths and shapes but the same height (Toraya, Yoshimura & Somiya, 1983; Howard & Snyder, 1983).

Some other functions that have been used include the double Gaussian [Fig. 2.3.3.9(*b*)] for low-resolution synchrotron data (Will, Masciocchi, Parrish & Hart, 1987), a Gaussian with shifted Lorentzian component to account for the asymmetry on the low-2θ side of the tail (Will, Masciocchi, Parrish & Lutz, 1990), profile modelling of single isolated peaks with a rational function, *e.g.* the ratio of two polynomials (Pyrros & Hubbard, 1983). In contrast to these analytical-type functions, some empirical functions have been developed. They are the 'learned' (experimental) peak-shape function (Hepp & Baerlocher, 1988) and the direct fitting of experimental data represented by Fourier series (Mortier & Constenoble, 1973).

The sum of Lorentzians has been used for X-ray tube focusing profiles (Parrish & Huang, 1980; Taupin, 1973). The instrument function $(\lambda * G)$ is determined (see below) by a sum of Lorentzian curves, three each for $K\alpha_1$ and $K\alpha_2$ and one for the weak $K\alpha_3$ satellite. Three Lorentzians were used to match the asymmetry although a greater or lesser number could be used depending on the profile symmetry. Each curve has three parameters (intensity, half-width at half-height, and peak position) and the 21 parameters are adjusted by the computer program to give the best fit to the experimental data, which may contain 150 to 300 points. This is done only once for each particular instrument set-up. After $(\lambda * G)$ is determined, the profile fitting is easy and fast because only the specimen contribution S must be convoluted with $(\lambda * G)$. If the specimen has no asymmetric broadening other than $(\lambda * G)$, S can be approximated by a single symmetrical Lorentzian for each reflection; a split Lorentzian can be used if there is asymmetric broadening.

A function can be tested using isolated profiles of a standard specimen such as silicon, tungsten, quartz, and others which have $< 10\,\mu$m particles and no specimen broadening (Fawcett *et al.*, 1988). It is necessary to do this test carefully and whenever the instrument parameters are changed.

The instrument function can be measured using isolated profiles of standard specimens as stated above. The measurements should be made with small $\Delta 2\theta \simeq 0.01^\circ$ steps and count times long enough to accumulate about 25 000 to 50 000 counts on the $K\alpha_1$ peaks for good counting statistics. By measuring a number of profiles separated by no more than about 5 to 10°, the instrument function can be established for the angular range of interest. A linear interpolation of the profile-fitting parameter between adjacent profiles gives a continuous function for use at any 2θ in the range. The

intensities of the derived profile parameters are normalized and stored in the computer for later use. Note that any change in the X-ray spectrum or instrument geometry requires another set of measurements. The instrument function is also an important aid in computer graphics as described in Subsection 2.3.3.9.

The fitting of conventional diffractometer profiles was considerably improved by the use of a convolution function, in which the Pearson VII function is convoluted with the observed instrument function (Toraya *et al.*, 1983; Toraya, 1988). Enzo, Fagherrazzi, Benedetti & Polizzi (1988; Benedetti, Fagherazzi, Enzo & Battagliarin, 1988) used the convolution of a pseudo-Voigt function as the true data function and the convolution of exponential and pseudo-Voigt functions as the instrumental function for crystallite size and strain analysis. These functions have advantages in analysing the crystallite size and strain, although they require longer computation time for calculating the convolution.

Background intensity is usually included in the refinement. A first- or second-order polynomial is used to represent the background function $B(x)$ in equation (2.3.3.12) in a small 2θ range, and the polynomial coefficients are adjusted during the least-squares refinement. In some cases, the background is subtracted from the pattern before the refinement by using the lowest intensities between the reflections. The background in the vicinity of high-intensity peaks and peak clusters is usually higher and should be avoided.

In the least-squares refinement, the following quantity is minimized:

$$\Delta = \sum_{i=1}^{N} w_i [Y(x_i)_{\rm obs} - Y(x_i)_{\rm calc}]^2, \qquad (2.3.3.17)$$

where N is the number of observations, w_i is the weight assigned to the ith observation, and $Y(x_i)_{\rm obs}$ is the observed profile intensity. A statistical weighting factor such as $w_i = \sigma_i^2$, where $\sigma_i^2 = 1/Y(x_i)_{\rm obs}$, is frequently used. The quality of the fitting procedure is generally expressed by R factors such as R_{wp}, the weighted R factor for profile intensity, which includes the entire scattering range and the background. The definitions of these factors are summarized by Young, Prince & Sparks (1982). The R_p and R_{wp} factors are given as

$$R_p(\%) = 100 \sum_{i=1}^{N} |Y(x_i)_{\rm obs} - Y(x_i)_{\rm calc}| \Big/ \sum_{i=1}^{N} Y(x_i)_{\rm obs}, \qquad (2.3.3.18)$$

$$R_{wp}(\%) = 100 \left\{ \frac{\sum_{i=1}^{N} w_i \left[Y(x_i)_{\rm obs} - Y(x_i)_{\rm calc}\right]^2}{\sum_{i=1}^{N} w_i Y(x_i)_{\rm obs}^2} \right\}^{1/2}. \qquad (2.3.3.19)$$

If the selected function is inappropriate, it will show up on the difference curve (experimental − calculated; see Fig. 2.3.3.9), and high R_p and R_{wp} factors.

A whole-powder-pattern fitting technique without using the structural model was proposed for analysing neutron powder data (Pawley, 1981) and then extended to X-ray data (Toraya, 1986). The method executes the whole pattern decomposition (*i.e.* fitting all the profiles) in one step. In this technique, the peak position T_j in equation (2.3.3.12) is a function of unit-cell parameters, and the unit-cell parameters are refined instead of individual peak positions. Furthermore, the angular dependence of the profile width can be expressed approximately as

$$w(2\theta) = \sqrt{w_1 + w_2 \tan\theta + w_3 \tan^2\theta}, \qquad (2.3.3.20)$$

where w_1, w_2, and w_3 are adjustable parameters (Caglioti, Paoletti & Ricci, 1958); but see also Louër & Langford (1988). The profile-shape dependency on 2θ is ignored when fitting a small 2θ range, but it must be taken into account in the whole-powder-pattern fitting in both focusing and parallel-beam geometries. The least-squares ill conditioning is handled by imposing the constraints on the peak positions in the profile-fitting procedure.

Approximate unit-cell parameters are required to start the refinement. Advantages of this technique are: (1) the unit-cell parameters are refined to high precision; (2) the analysis is rapid and straightforward; (3) it is also powerful in analysing complex powder patterns. The output of indices and integrated intensities of all reflections can be used to calculate Patterson and Fourier diagrams, and thus used for *ab initio* structure determination (McCusker, 1988) and the structure refinement based on the integrated intensities such as used in the *POWLS* program (Will, 1979).

The convolution equation is used in place of $P(x)$ in equation (2.3.3.12), in which the true data function represented by a pseudo-Voigt or Pearson VII has adjustable parameters of crystallite size and strain (Toraya, 1989). The anisotropic crystallite size assuming cylindrical shape has been determined by whole-powder-pattern fitting for complex powder patterns.

The advantage of profile fitting is illustrated in Fig. 2.3.3.10 for the quartz cluster at 68° with Cu $K\alpha$ where the doublet separation is 0.19° and the FWHM is 0.14°. The relative intensities of the 122, 203, and 301 $K\alpha_1$ peaks are 81:97:100, which differ from the profile-fitted peaks, 90:100:67, due to the overlapping. The sum of the fitted curves is the solid line which passes through the experimental points. The peak-search (or strip-chart) intensities that are not corrected for overlaps are more likely to correspond to the ICDD powder file than the profile-fitted values. Profile fitting is capable of about $\pm 0.0004°2\theta$ and 0.2% intensity for good experimental data (Parrish & Huang, 1980). Even in data with poor counting

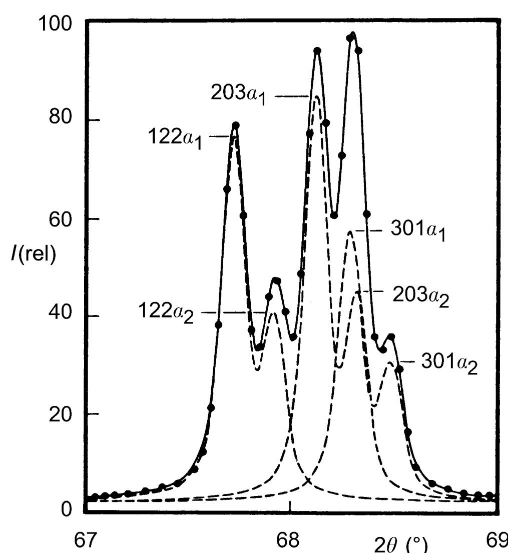

Fig. 2.3.3.10. Profile fitting with sum-of-Lorentzians method. Individual reflections shown as dashed-line curves and sum as solid line passing through experimental points. Quartz peak cluster, Cu $K\alpha_1$, $K\alpha_2$, conventional diffractomer.

statistical accuracy, it is possible to identify very weak peaks with low P/B as shown in Fig. 2.3.3.11.

2.3.3.9. *Computer graphics for powder patterns*

An interactive graphics display program is a very important asset for interpreting and analysing powder diffraction data. If a colour graphics station is used, the display can be enhanced by using various colours. The simplest form is the VDU display of experimental points connected with straight lines, which appears similar to a strip-chart recording but has no time-constant error and is printed on page-size paper. It avoids storing large numbers of charts because hundreds of patterns can be stored on a diskette and displayed and printed at any time.

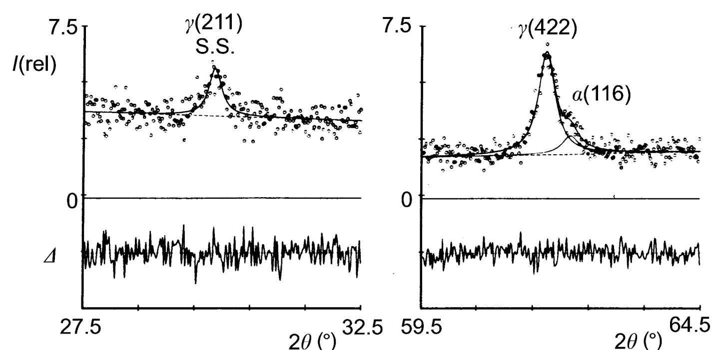

Fig. 2.3.3.11. Profile fitting of poor statistical data.

The basic parameters required in one of the published methods (Parrish, Huang & Ayers, 1984) are the d's and I's of the reflections, the wavelength and profile shapes ($\lambda * G$ instrument function). This makes it possible to produce a pattern exactly as it would appear on the user's diffractometer, aside from contributions arising from sample microstructure. The step size can be included if experimental patterns are to be reproduced or if patterns are to be subtracted. A section of the pattern can be enlarged to the full screen size by entering the desired angular range and highest peak intensity. A linear background can be added by entries at the low- and high-2θ points. Nonlinear background, *e.g.* from an amorphous substrate, can be transferred from a stored file. Counting statistical noise can be added to a simulated pattern by using a normally distributed random number with a standard deviation scaled to the calculated $I^{1/2}$. Noise in an experimental pattern can be smoothed. A profile broadening factor can be added to the $\lambda * G$ function. Quantitative synthesis of a mixture can be simulated by entering the relative weight percentage and reference intensity, the ratio of the intensities of the strongest lines of each pattern in a 50–50 mixture, or the ICDD values compared to α-Al_2O_3 (de Wolff & Visser, 1988; Davis & Smith, 1988). The program has access to the ICDD file stored on disk so that any card can be reproduced as a pattern using any wavelength. Some examples are shown in Fig. 2.3.3.12.

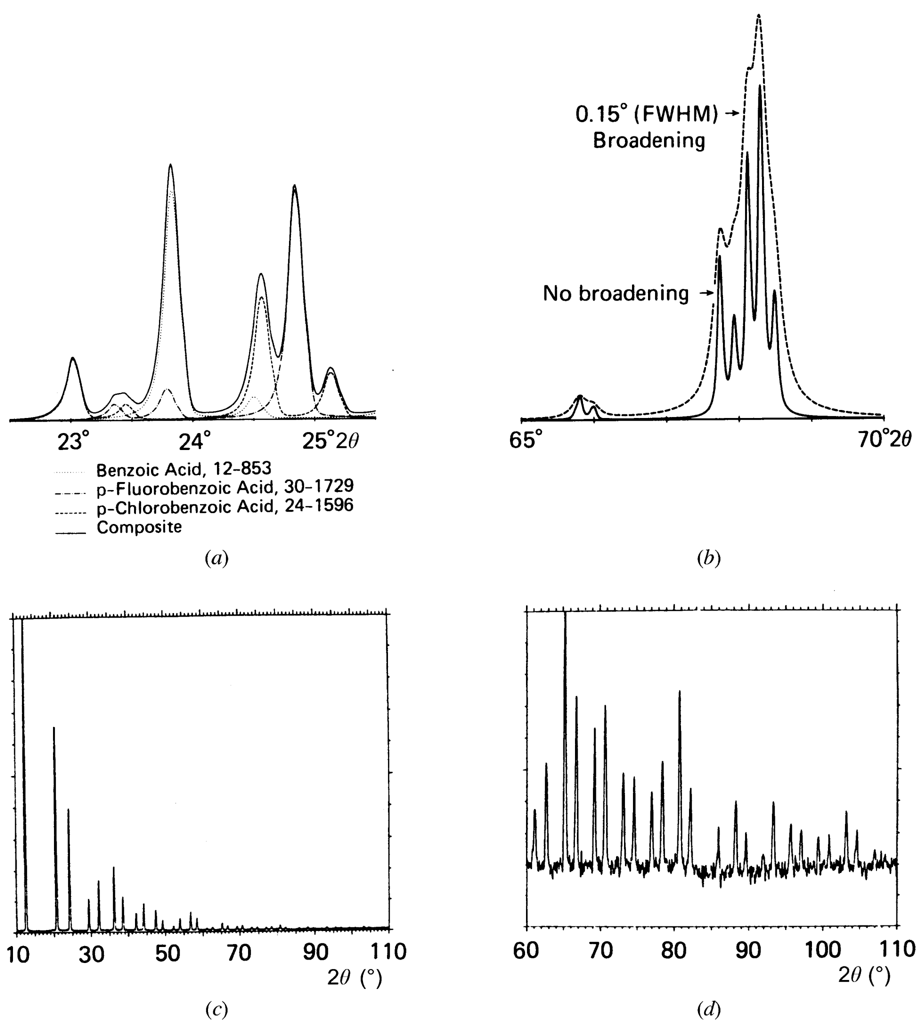

Fig. 2.3.3.12. Some examples of computer graphics of powder patterns. (*a*) Overlay of three patterns with ICDD card numbers. (*b*) Effect of adding 0.15° to FWHM. (*c*) Synchrotron 0.6888 Å radiation pattern of Si powder. (*d*) Low-intensity section enlarged and 11-point smoothing.

references